

InP-Based Photodetectors Monolithically Integrated with 90° Hybrid toward Over 400 Gb/s Coherent Transmission Systems

Hideki YAGI^{†a)}, Senior Member, Takuya OKIMOTO^{††}, Member, Naoko INOUE[†], Koji EBIHARA^{††}, Nonmembers, Kenji SAKURAI^{††}, Member, Munetaka KUROKAWA[†], Satoru OKAMOTO^{††}, Kazuhiko HORINO^{††}, Tatsuya TAKEUCHI^{††}, Kouichiro YAMAZAKI^{††}, Yoshifumi NISHIMOTO^{††}, Yasuo YAMASAKI^{††}, Mitsuru EKAWA^{†,††}, Masaru TAKECHI[†], Nonmembers, and Yoshihiro YONEDA^{††}, Member

SUMMARY We present InP-based photodetectors monolithically integrated with a 90° hybrid toward over 400 Gb/s coherent transmission systems. To attain a wide 3-dB bandwidth of more than 40 GHz for 400 Gb/s dual-polarization (DP)-16-ary quadrature amplitude modulation (16 QAM) and 600 Gb/s DP-64 QAM through 64 GBaud operation, a p-i-n photodiode structure consisting of a GaInAs thin absorption and low doping n-typed InP buffer layers was introduced to overcome the trade-off between short carrier transit time and low parasitic capacitance. Additionally, this InP buffer layer contributes to the reduction of propagation loss in the 90° hybrid waveguide, that is, this approach allows a high responsivity as well as wide 3-dB bandwidth operation. The coherent receiver module for the C-band (1530 nm – 1570 nm) operation indicated the wide 3-dB bandwidth of more than 40 GHz and the high receiver responsivity of more than 0.070 A/W (Chip responsivity within the C-band: 0.130 A/W) thanks to photodetectors with this photodiode design. To expand the usable wavelengths in wavelength-division multiplexing toward large-capacity optical transmission, the photodetector integrated with the 90° hybrid optimized for the L-band (1565 nm – 1612 nm) operation was also fabricated, and exhibited the high responsivity of more than 0.120 A/W over the L-band. Finally, the InP-based monolithically integrated photonic device consisting of eight-channel p-i-n photodiodes, two 90° hybrids and a beam splitter was realized for the miniaturization of modules and afforded the reduction of the total footprint by 70% in a module compared to photodetectors with the 90° hybrid and four-channel p-i-n photodiodes.

key words: digital coherent transmission, InP, 90° hybrid, multimode interference structure, p-i-n photodiode

1. Introduction

The expansion of video streaming services and mobile terminals has continuously promoted the significant increase of data traffic, and it has accelerated the development of high-speed and large-capacity transmission. To cope with this demand, the digital coherent transmission technology using spectrally-efficient modulation formats, such as quadrature phase-shift keying (QPSK) and quadrature amplitude modulation (QAM) has been widely adopted for not only long-haul networks but also metropolitan area networks [1]–[4]. High port density which drives the miniaturization of optical components and low power dissipation is indispensable for

cost-sensitive metro and data center interconnect applications, and the downsizing of a coherent receiver is inevitable for pluggable transceivers with a smaller footprint and lower power dissipation, like a 100 Gb/s form-factor pluggable (CFP/CFP2) transceiver. The downsizing of a 90° hybrid waveguide for compact coherent receivers has been investigated through various approaches, such as the silica-based planar lightwave circuit (PLC), Silicon-photonics and InP-based monolithic integration technologies [5]–[10]. The InP-based monolithic integration of the 90° hybrid and p-i-n photodiodes can offer the elimination of complicated alignments in the assembly process as well as a smaller footprint in packaging, resulting in low production costs and the stabilization of receiver performance with mature process technologies [11]. We have demonstrated the 32 GBaud compact coherent receiver module using InP-based photodetectors which have the high responsivity through the butt-joint (BJ) coupling structure consisting of the 90° hybrid and four-channel p-i-n photodiodes [12]–[14]. In fact, this InP-based receiver has exhibited higher responsivity than that of InP-based receivers with the evanescent coupling structure consisting of the 90° hybrid and photodiodes [15] and receivers with the PLC-based 90° hybrid [7] thanks to the high optical coupling efficiency of the BJ coupling structure.

Furthermore, digital coherent transmission is very promising for over 400 Gb/s transmission systems in short-haul networks (Transmission distance: 10 – 100 km) including data center interconnect networks in addition to long-haul and metropolitan area networks [16]. InP-based photodetectors are very attractive for a wide 3-dB bandwidth of more than 40 GHz toward 400 Gb/s dual-polarization (DP)-16 QAM and 600 Gb/s DP-64 QAM with 64 GBaud operation [17], [18]. Although the wide bandwidth operation of photodiodes causes the decline of responsivity owing to the reduction of an absorber volume, photodiode design which is compatible with the wide 3-dB bandwidth and high responsivity is strongly required to improve the minimum receiver sensitivity of signal light for pluggable transceivers with low power dissipation.

In this paper, we report InP-based photodetectors monolithically integrated with the 90° hybrid toward 400 Gb/s and beyond coherent transmission systems using 64 GBaud operation. The outline of this paper is organized as follows. Section 2 discusses photodiode design to be

Manuscript received August 7, 2018.

Manuscript revised December 4, 2018.

[†]The authors are with Transmission Devices Laboratory, Sumitomo Electric Industries, Ltd., Yokohama-shi, 244–8588 Japan.

^{††}The authors are with Sumitomo Electric Device Innovations, Inc., Yokohama-shi, 244–0845 Japan.

a) E-mail: yagi-hideki@sei.co.jp

DOI: 10.1587/transele.2018ODI0006

compatible with the high responsivity and wide bandwidth operation and presents the properties of the photodetector integrated with the 90° hybrid for 64 GBaud operation. To expand the usable wavelengths in wavelength-division multiplexing as one of the approaches to large-capacity optical transmission [19], the photodetector for L-band operation is also discussed in Sect. 3. The monolithically integrated photonic device with eight-channel p-i-n photodiodes, two 90° hybrids and a beam splitter is exhibited for the miniaturization of modules in Sect. 4. Finally, we summarize and give conclusions of this paper in Sect. 5. The measurement condition, such as bias voltage of the responsivity and small-signal optical/electrical response in this paper was carried out in accordance with the specification of each receiver module.

2. Wide Bandwidth and High Responsivity Photodetectors Integrated with 90° Hybrid

2.1 Device Design

Figure 1 shows (a) the photomicrograph, (b) the schematic diagram of the 90° hybrid and (c) cross-sectional scanning electron microscope (SEM) images of spot-size converter (SSC), 90° hybrid and p-i-n photodiode sections for the InP-based photodetector monolithically integrated with the 90° hybrid [13], [14]. The chip size was $4.1\text{ mm} \times 1.6\text{ mm}$. The 90° hybrid is comprised of the 2×4 multimode interference structure (MMI) functioning as a 180° hybrid for in-phase relation, the 45° phase shifter and 2×2 MMI functioning for quadrature phase relation as shown in Fig. 1 (b). In this 90° hybrid design, the In-phase channels (CH-1 and CH-2) and the Quadrature channels (CH-3 and CH-4) are not spatially separated unlike that based on 4×4 MMI [20]. As a

result, the output channels from the 90° hybrid waveguide can be directly connected to 4-channel p-i-n photodiodes without waveguide intersections, which induce excess optical loss and crosstalk. Compact MMI design which has the narrower MMI width and shorter MMI length was adopted, since it was very effective for the reduction of the wavelength dependence of excess optical loss due to MMIs [21]. The asymmetric waveguide phase shifter (AWPS) with the delayed waveguide in one side of the Quadrature channels was adopted as the 45° phase shifter, because this structure allows the phase shift exploiting the difference of the optical path length without the precise control of a waveguide width (equivalent refractive index). Hence, AWPS affords larger tolerance in waveguide width variation compared with the phase shifter exploiting the difference of the waveguide width [22]. Furthermore, in order to suppress the frequency dependence of the common mode rejection ratio (CMRR), the waveguide layout of the In-phase and Quadrature channels was designed by considering the reduction of skew in the 90° hybrid, and skew was almost negligible in this 90° hybrid structure, which was estimated to be less than 0.5 ps by theoretical analysis.

A buried heterostructure (BH) layer was selectively formed in photodiode sections to reduce the dark current and in SSC sections to achieve the high optical coupling efficiency between the free space optics of a module, such as a polarization beam splitter (PBS) and a beam splitter (BS) and the 90° hybrid using the selective embedding regrowth technique. The low dark current of less than 5.0 pA at a reverse bias voltage of 3 V was obtained thanks to the reduction of the surface recombination at sidewalls of the deep-ridge stripe by the BH structure [23]. The difference of the dark current was also not observed in C-band and L-band photodiode design. In addition, the SSC core width was optimized to acquire optical coupling efficiency of more than 90% for an optical field consisting of the parallel Gaussian beam in horizontal and vertical directions, which corresponds to the mode field diameter (MFD) of $1.8\ \mu\text{m}$ from the optical configuration with lens optical coupling in the receiver module. This MFD was optimized in accordance with vertical MFD which is restricted by the thickness of the upper InP cladding layer for the SSC section. On the other hand, the deep-ridge waveguide without the InP embedding regrowth was maintained for the reduction of wavelength dependence of excess optical loss and for precise phase control in the 90° hybrid consisting of MMIs.

2.2 Photodiode Design for Wide Bandwidth Operation

In order to realize high-speed p-i-n photodiodes toward 64 GBaud operation, short carrier transit time and low parasitic capacitance in the photodiode are essential. Although a thinner absorption layer is required to obtain shorter carrier transit time, this approach causes the increase of parasitic capacitance in the photodiode. To overcome the trade-off between the two dominant factors, the low doping n-typed (n^-)-InP buffer layer ($N_D < 1 \times 10^{17}\ \text{cm}^{-3}$) was introduced

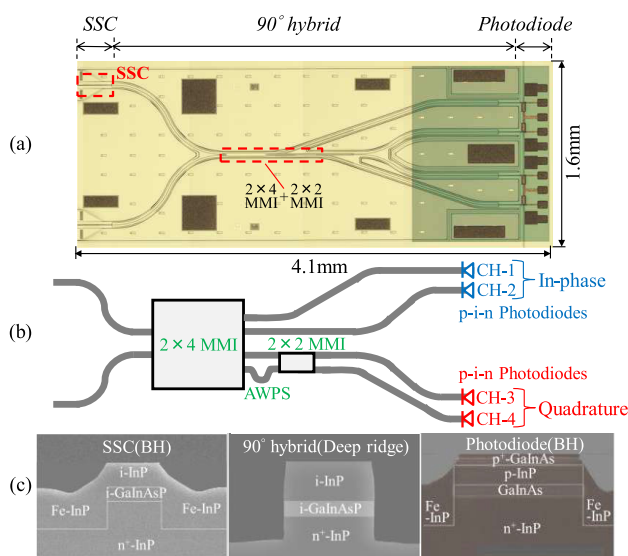


Fig. 1 (a) Photomicrograph, (b) schematic diagram of the 90° hybrid and (c) cross-sectional SEM images of SSC, 90° hybrid and photodiode sections for the InP-based photodetector monolithically integrated with the 90° hybrid.

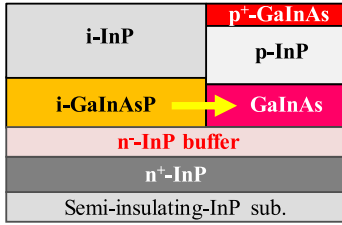


Fig. 2 Schematic cross-sectional view of propagation direction for photodetectors monolithically integrated with the 90° hybrid.

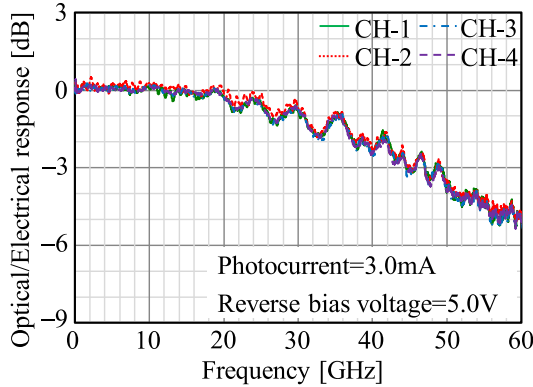


Fig. 3 Optical/Electrical response of the photodetector monolithically integrated with the 90° hybrid for 64 GBaud under the optical input power condition of 3 mA at a reverse bias voltage of 5.0 V.

between absorption (GaInAs) and high doping n-typed (n^+ -InP) contact layers in the p-i-n photodiode structure. This n^- -InP buffer layer keeps down the decrease in the width of the depletion layer and allows the compatibility of short carrier transit time and low parasitic capacitance in the p-i-n photodiode. As a result, parasitic capacitance of the p-i-n photodiode was around 35 fF at a reverse bias voltage of 5 V, that is, it's the improvement of 15 fF compared with the photodiode design for 32 GBaud operation [12]. In addition, the n^- -InP buffer layer lies under the core layer (i-GaInAsP) of the 90° hybrid as shown in Fig. 2 and contributes to the suppression of free carrier absorption loss due to the high doping of the n^+ -InP contact layer, that is, this waveguide structure compensates the decline of quantum efficiency caused by the designed thinner absorption layer for high-speed response. Hence, the optical propagation loss of this structure (0.06 dB/mm) was improved as compared with that of the previous structure (0.15 dB/mm) [24], and high responsivity was achieved with the decrease of optical propagation loss in the 90° hybrid waveguide as well as wide bandwidth operation through this n^- -InP buffer layer [14], [25].

2.3 Device Performance

The fabrication process of the InP-based photodetector monolithically integrated with the 90° hybrid using BJ and selective embedding regrowth processes was fully described in Ref. [12]–[14] and Sect. 4.1. Figure 3 shows the small-signal optical/electrical response of the photodetector integrated with the 90° hybrid for 64 GBaud operation. The

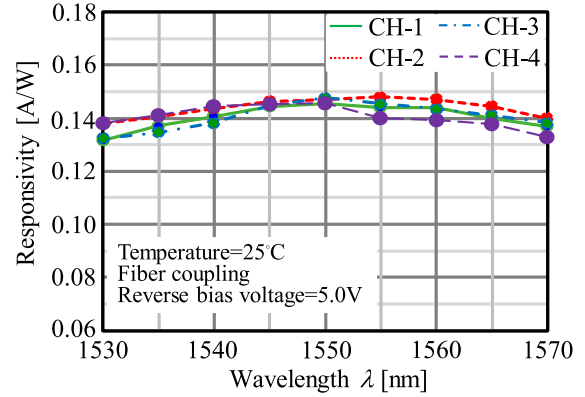


Fig. 4 The wavelength dependence of responsivity for the photodetector monolithically integrated with the 90° hybrid. Responsivity over the C-band was measured under a reverse bias voltage of 5.0 V at a temperature of 25°C.

wide 3-dB bandwidth of more than 46 GHz was achieved for four-channel p-i-n photodiodes under high optical input power condition (3 mA) at a reverse bias voltage of 5.0 V thanks to the p-i-n photodiode design with the thin absorption layer and the n^- -InP buffer layer.

Figure 4 shows the wavelength dependence of the responsivity for the photodetector integrated with the 90° hybrid at a reverse bias voltage of 5.0 V over the C-band. The responsivity at a wavelength of 1550 nm including the hybrid splitting loss of 6.0 dB (intrinsic loss), the optical propagation loss of 0.4 dB and the fiber coupling loss (w/ AR coating) of 1.5 dB was as high as 0.146 A/W in the average of four-channel photodiodes, and the responsivity of higher than 0.130 A/W was acquired over the C-band. This high responsivity was achieved through the decrease of propagation loss using the n^- -InP buffer layer in addition to high optical coupling efficiency with the BJ coupling structure consisting of the 90° hybrid and p-i-n photodiodes. In fact, the responsivity including the fiber coupling loss of 1.5 dB for the discrete waveguide photodiode with the BJ interface (w/o 90° hybrid) was 0.64 A/W at a wavelength of 1550 nm. From this result, we assume that excess optical loss at the interface of the BJ regrowth is less than 0.5 dB. The responsivity imbalance of the In-phase and Quadrature channels was also less than ± 0.5 dB over the C-band through small loss imbalance of the 90° hybrid consisting of 2×4 MMI, AWPS working as the 45° phase shifter and 2×2 MMI.

2.4 Receiver Module Performance

Figure 5 shows (a) the schematic diagram and (b) the photograph for a fabricated polarization and phase diversity intradyne coherent receiver (ICR) module [14], [17], [19]. The package body size is 12.0 mm \times 22.7 mm \times 4.5 mm, and it is small enough to install components into pluggable coherent transceivers, such as CFP/CFP2.

Optical couplings between optical fibers and 90° hybrids are constructed with free space optics as shown in Fig. 5 (a). Signal light propagating from a single mode fiber

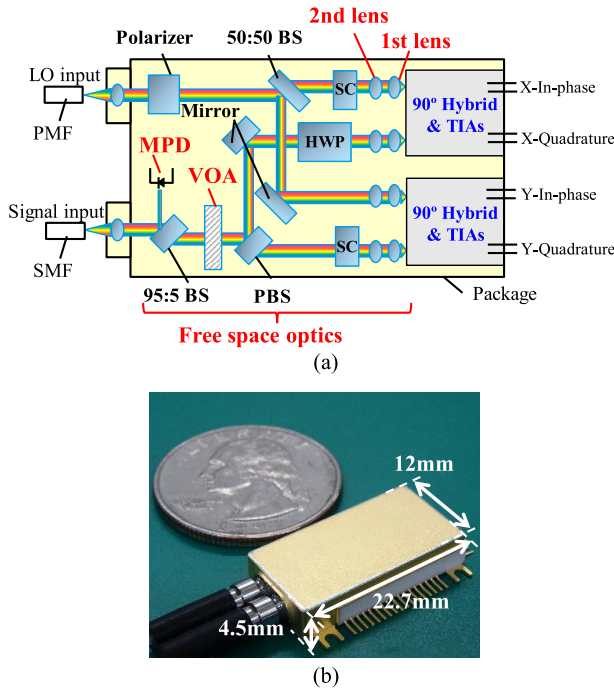


Fig. 5 (a) Schematic diagram and (b) photograph for a fabricated polarization and phase diversity intradyne coherent receiver module using InP-based photodetectors monolithically integrated with the 90° hybrid.

(SMF) is converted to collimated light by a collimator lens. A small portion (5%) of the signal light is split to the monitor photodiode (MPD) with BS. Then, the signal light is decomposed to TE polarized light and TM polarized light by PBS. The TE polarized light is coupled to the 90° hybrid for Y-polarization through the lens. The TM polarized light is converted to TE polarized light using the half-wave plate (HWP). This TE polarized light is coupled to the 90° hybrid for X-polarization through the lens.

The local oscillator (LO) light is also launched to the receiver through a polarization maintaining fiber (PMF). The LO light from PMF is coupled to the collimate lens, and this light is split with BS. The LO light is coupled to the 90° hybrid for X-polarization and that for Y-polarization through the lens. A lens unit consisting of 2nd Lens and 1st Lens was adopted as shown in Fig. 5(a), since it has advantages for broadening the tolerance of lens alignment thanks to designing a combination of the focal length for 1st Lens and that for 2nd Lens. The variable optical attenuator (VOA) was located between PBS and 95:5-BS. Skew controller (SC) was used to compensate the difference of light path length between X- and Y-polarization.

Figure 6 shows the small-signal optical/electrical response for the coherent receiver module using photodetectors monolithically integrated with the 90° hybrid [14], [17]. The 3-dB bandwidth of more than 40 GHz was confirmed as the output of SiGe-based trans-impedance amplifiers (TIAs) which has the transimpedance of 5 k Ω . Additionally, even though the intrinsic loss of 3 dB was caused by the separation of TE polarized light and TM polarized

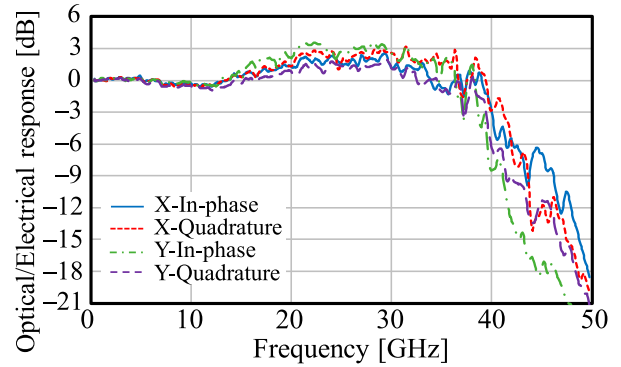


Fig. 6 Small-signal optical/electrical response for the coherent receiver module using InP-based photodetectors monolithically integrated with the 90° hybrid. The photodiode reverse bias voltage and TIA power supply voltage were +5.0 V and +3.3 V, respectively.

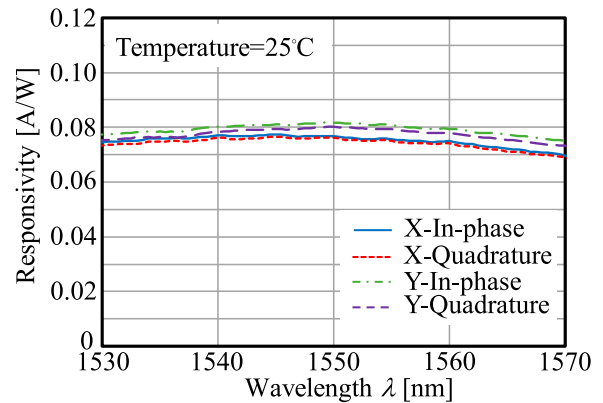


Fig. 7 Wavelength dependence of the responsivity at a temperature of 25°C for the coherent receiver module using InP-based photodetectors monolithically integrated with the 90° hybrid.

light in PBS, the receiver responsivity which is the average of two photodiodes in X-In-phase, X-Quadrature, Y-In-phase and Y-Quadrature was higher than 0.070 A/W over the C-band with the introduction of SSC as shown in Fig. 7, [14], [17]. Hence, these results revealed that this InP-based photodetector is very useful for coherent receiver modules with 64 GBaud operation toward 400 Gb/s DP-16 QAM and 600 Gb/s DP-64 QAM.

3. Expansion of Operation Wavelength to the L-Band

Although a responsivity declines due to a low absorption coefficient in the wavelength range of longer than 1600 nm even in photodiodes using a GaInAs absorption layer, the expansion of operation wavelength to the L-band (1565 nm to 1612 nm) has been discussed toward the further increase of data traffic, since higher order QAM with the higher optical-signal-to-noise-ratio (OSNR) has affected transmission distance [19]. In order to achieve the high responsivity over the L-band, the design of 2 \times 4 MMI, 2 \times 2 MMI and the 45° phase shifter which are components for the 90° hybrid was optimized to obtain high transmittance and small loss imbalance over the L-band. Furthermore, the bandgap

edge of the GaInAs layer becomes close to the longer wavelength of the L-band. Especially, the absorption coefficient of the GaInAs layer steeply decreases in the low temperature range. To compensate for the degradation of the absorption coefficient, we optimized the length of the absorption layer along the propagation direction as shown in Fig. 2, that is, the same thickness in the absorption layer was adopted for C- and L- bands.

The responsivity over C- and L-bands for the waveguide photodiode without the 90° hybrid (total length of photodiode and waveguide sections: 0.9 mm) fabricated using BJ regrowth was evaluated at temperatures of -5°C and 25°C. Figure 8 shows the wavelength dependence of the responsivity normalized by that for a wavelength of 1615 nm at a temperature of 25°C. The normalized responsivity at temperatures of -5°C and 25°C was almost constant over C- and L-bands thanks to the optimization in the length of the absorption layer.

Figure 9 shows the wavelength dependence of the responsivity for the photodetector integrated with the 90° hybrid at a reverse bias voltage of 1.6 V over the L-band. All-

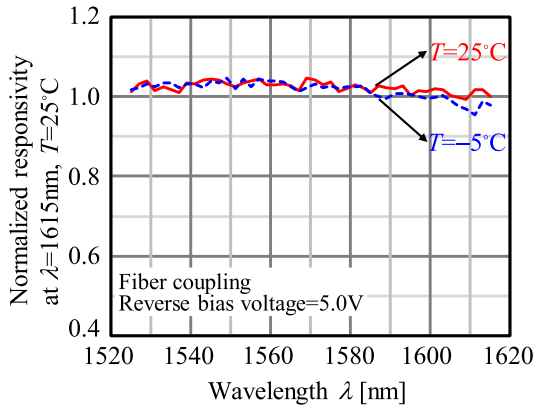


Fig. 8 The wavelength dependence of the responsivity normalized by that for a wavelength of 1615 nm at a temperature of 25°C. The responsivity of the waveguide photodiode without the 90° hybrid was measured at temperatures of -5°C and 25°C.

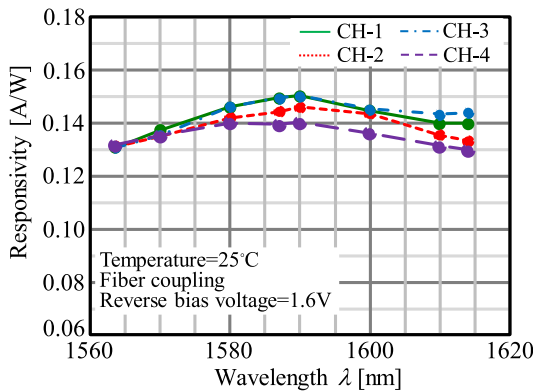


Fig. 9 The wavelength dependence of responsivity for the photodetector monolithically integrated with the 90° hybrid. Responsivity over the L-band was measured under a reverse bias voltage of 1.6 V at a temperature of 25°C.

though the responsivity is affected by the 90° hybrid consisting of MMIs which has the peak wavelength of 1590 nm in transmittance, the responsivity at a wavelength of 1590 nm including the hybrid splitting loss of 6.0 dB (intrinsic loss), the optical propagation loss of 0.4 dB and the fiber coupling loss (w/ AR coating) of 1.5 dB was as high as 0.147 A/W in the average of four-channel photodiodes, and the responsivity of higher than 0.120 A/W was successfully achieved over the L-band. The responsivity imbalance of the In-phase and Quadrature channels was also less than ±0.5 dB over the L-band.

Moreover, by the introduction of the high-speed photodiode design concept represented in Sect. 2.2, the 3-dB bandwidth of more than 40 GHz for 64 GBaud operation was accomplished over the L-band [19].

4. 8-ch p-i-n Photodiodes Integrated with 90° Hybrids

4.1 Device Design & Fabrication Process

Toward the further miniaturization of modules, such as IC-TROSA (Integrated Coherent Transmitter-Receiver Optical Sub-Assembly) for the next generation pluggable transceiver, a monolithically integrated photonic device consisting of SSC, BS, two 90° hybrids and eight-channel (8-ch) p-i-n photodiodes was fabricated for a smaller footprint in packaging. Figure 10 shows (a) the photomicrograph and (b) the schematic diagram of 90° hybrids for this integrated photonic device. 90° hybrids for X- and Y-channels are comprised of 2 × 4 MMI for the In-phase channels (I-CH), 2 × 2 MMI for the Quadrature channels (Q-CH) and the 45° phase shifter, respectively. On the input side of LO, 1 × 2 MMI was located as BS.

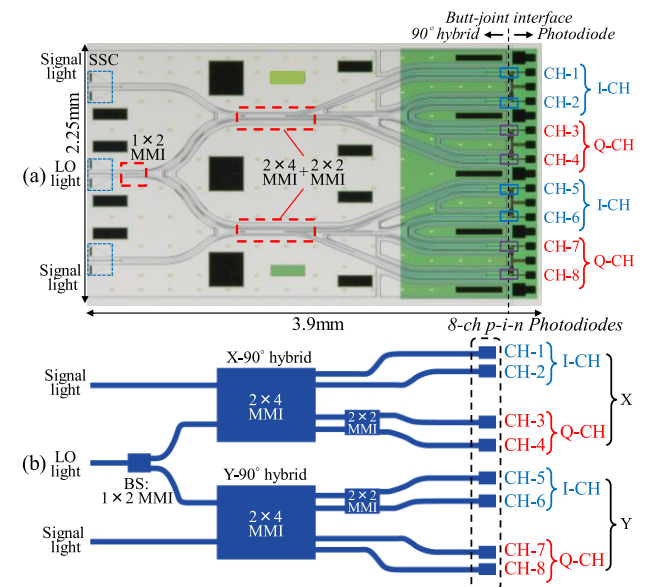


Fig. 10 (a) Photomicrograph and (b) schematic diagram of the completed InP-based monolithically integrated photonic device consisting of SSC, BS, two 90° hybrids and 8-ch p-i-n photodiodes.

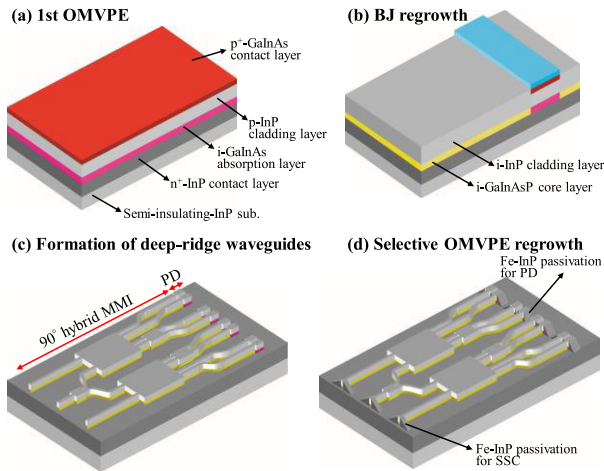


Fig. 11 Fabrication process of the InP-based monolithically integrated photonic device consisting of SSC, BS, two 90° hybrids and 8-ch p-i-n photodiodes.

Figure 11 shows the fabrication process of this integrated photonic device. A p-i-n photodiode structure with a GaInAs absorption layer was prepared on a semi-insulating 3-inch InP wafer by organometallic vapor-phase-epitaxial (OMVPE) growth [Fig. 11 (a)]. The waveguide section with the GaInAsP core layer and the photodiode section were combined using the BJ regrowth process [Fig. 11 (b)]. Deep-ridge waveguide stripes for SSC, BS, 90° hybrid and photodiode sections were simultaneously formed by standard optical i-line stepper lithography and reactive ion etching (RIE) techniques [Fig. 11 (c)]. Fe-doped InP-BH layers were selectively formed to reduce the dark current in photodiode sections and to obtain optical coupling efficiency over 90% between the free space optics of a module and input waveguides of this integrated photonic device in SSC sections using OMVPE regrowth techniques [Fig. 11 (d)]. Although a relatively thin InP passivation layer was adopted in the photodiode section to suppress parasitic capacitance for a high-speed response, a thicker InP passivation layer was formed in the SSC section to acquire target MFD. Hence, the wider selective regrowth mask compared with that of the photodiode section was arranged on the terrace part in the side of the SSC waveguide [23]. Then, electrodes were evaporated for the p- and n-side ohmic contacts, followed by an anti-reflection (AR) coating on the optical input facet.

The chip size was $3.9 \text{ mm} \times 2.25 \text{ mm}$, and this monolithically integrated photonic device with various functionalities enables the reduction of the total footprint by 70% in a module as compared with that using previously reported 4-ch p-i-n photodiodes integrated with the 90° hybrid [12]–[14].

4.2 Device Performance

Figure 12 shows dark current and reverse bias voltage characteristics of each channel. The dark current at a reverse bias voltage of 5.0 V was as low as approximately 10 pA for all 8-ch p-i-n photodiodes. This result indicates that no no-

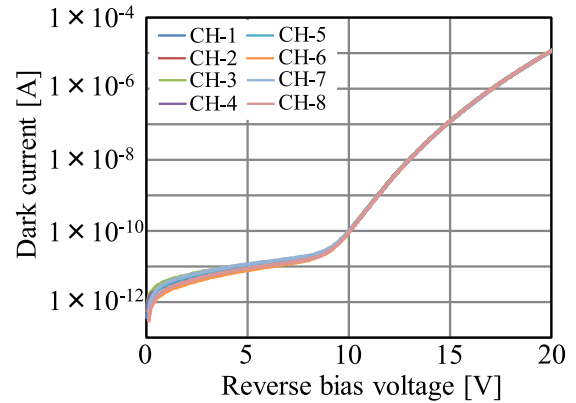


Fig. 12 Dark current-reverse bias voltage characteristics of 8-ch p-i-n photodiodes monolithically integrated with 90° hybrids.

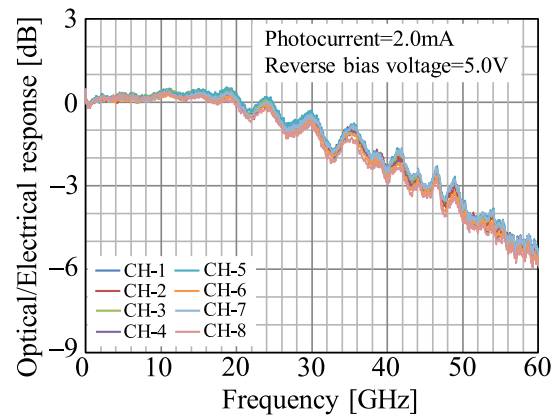


Fig. 13 Optical/Electrical response of 8-ch p-i-n photodiodes monolithically integrated with 90° hybrids under optical input power condition of 2.0 mA at a reverse bias voltage of 5.0 V.

ticeable leakage current was caused through the monolithic integration process of 90° hybrid waveguides and 8-ch p-i-n photodiodes using BJ regrowth.

The responsivity of 8-ch p-i-n photodiodes including the hybrid splitting loss of 6.0 dB (intrinsic loss), the optical propagation loss of 0.4 dB and the fiber coupling loss (w/ AR coating) of 1.5 dB was more than 0.110 A/W over the C-band at a reverse bias voltage of 5.0 V, that is, this value is sufficient for receiver modules. The responsivity at a wavelength of 1550 nm was as high as 0.141 A/W in the average of 8-ch p-i-n photodiodes. The responsivity imbalance of I-CH and Q-CH for both X- and Y-channels was also less than ± 0.5 dB over the C-band through highly uniform deep-ridge waveguides using dry etching processes and small loss imbalance of the 90° hybrid consisting of MMIs.

With respect to BS consisting of 1×2 MMI, the difference of the responsivity between signal input and LO input ports was 3.0 ± 0.2 dB over the C-band, and it has sufficient property as a 3 dB coupler for BS.

The small-signal optical/electrical response of the integrated photonic device was evaluated as shown in Fig. 13. The wide 3-dB bandwidth of 43 GHz was obtained in all 8-ch p-i-n photodiodes under high optical input power con-

dition (Photocurrent: 2 mA) at a reverse bias voltage of 5.0 V. Consequently, these results indicate that this monolithically integrated photonic device has adequate properties toward the realization of small-footprint modules with 64 GBaud operation for 400 Gb/s DP-16 QAM and 600 Gb/s DP-64 QAM.

5. Conclusions

We demonstrated InP-based photodetectors monolithically integrated with the 90° hybrid toward over 400 Gb/s coherent transmission systems. Coherent receiver modules for 64 GBaud operation indicated the wide 3-dB bandwidth (> 40 GHz) and the high receiver responsivity over the C-band (> 0.070 A/W) thanks to the photodetector with p-i-n photodiode design to be compatible with the high responsivity and wide 3-dB bandwidth operation.

The photodetector integrated with the 90° hybrid optimized for the L-band operation exhibited the high responsivity (> 0.120 A/W) even in the wavelength range of longer than 1600 nm.

Finally, the InP-based monolithically integrated photonic device consisting of 8-ch p-i-n photodiodes, two 90° hybrids and BS allowed the reduction of the total footprint for receiver modules in addition to good photodiode characteristics. From these results, we substantiated that the InP-based photodetector presents high performance and is very effective for future coherent transmission systems using over 400 Gb/s operation and pluggable transceivers.

References

- [1] S. Tsukamoto, D.-S. Ly-Gagnon, K. Katoh, and K. Kikuchi, "Coherent Demodulation of 40-Gbit/s Polarization-Multiplexed QPSK Signals with 16-GHz Spacing after 200-km Transmission," Proc. OFC/NFOEC 2005, Anaheim, CA, paper PDP29, pp.1–3, March 2005.
- [2] G. Charlet, J. Renaudier, H. Mardoyan, P. Tran, O. Bertran Pardo, F. Verluise, M. Achouche, A. Boutin, F. Blache, J.-Y. Dupuy and S. Bigo, "Transmission of 16.4Tbit/s Capacity over 2,550km using PDM QPSK Modulation Format and Coherent Receiver," Proc. OFC/NFOEC 2008, San Diego, CA, paper PDP3, pp.1–3, Feb. 2008.
- [3] S. Oda, T. Tanimura, T. Hoshida, C. Ohshima, H. Nakashima, Z. Tao, and J.C. Rasmussen, "112 Gb/s DP-QPSK Transmission Using a Novel Nonlinear Compensator in Digital Coherent Receiver," Proc. OFC/NFOEC 2009, San Diego, CA, paper OThR6, pp.1–3, March 2009.
- [4] B. Zhang, C. Malouin, and T.J. Schmidt, "Towards full band colorless reception with coherent balanced receivers," Opt. Express, vol.20, no.9, pp.10339–10352, April 2012.
- [5] H.-G. Bach, A. Matiss, C.C. Leonhardt, R. Kunkel, D. Schmidt, M. Schell, and A. Umbach, "Monolithic 90° Hybrid with Balanced PIN Photodiodes for 100 Gbit/s PM-QPSK Receiver Applications," Proc. OFC/NFOEC 2009, San Diego, CA, paper OMK5, pp.1–3, March 2009.
- [6] Y. Painchaud, M. Pelletier, M. Poulin, F. Pelletier, C. Latrasse, G. Robidoux, S. Savard, J.-F. Gagné, V. Trudel, M.-J. Picard, P. Poulin, P. Sirois, F. D' Amours, D. Asselin, S. Paquet, C. Paquet, M. Cyr, M. Guy, M. Morsy-Osman, Q. Zhuge, X. Xu, M. Chagnon, and D.V. Plant, "Ultra-Compact Coherent Receiver Based on Hybrid Integration on Silicon," Proc. OFC/NFOEC 2013, Anaheim, CA, paper OM2J.2, pp.1–3, March 2013.
- [7] M. Itoh and Y. Kurata, "Heterogeneous integration of InP PDs on Silica-based PLCs," Proc. OFC/NFOEC 2013, Anaheim, CA, paper OTh3H.4, pp.1–3, March 2013.
- [8] C. Doerr, L. Chen, D. Vermeulen, T. Nielsen, S. Azemati, S. Stulz, G. McBrien, X.-M. Xu, B. Mikkelsen, M. Givehchi, C. Rasmussen, and S.-Y. Park, "Single-Chip Silicon Photonics 100-Gb/s Coherent Transceiver," Proc. OFC/NFOEC 2014, San Francisco, CA, PDP paper Th5C.1, pp.1–3, March 2014.
- [9] M. Takahashi, Y. Uchida, S. Yamasaki, J. Hasegawa, and T. Yagi, "Compact and Low-Loss Coherent Mixer Based on High Δ ZrO₂-SiO₂ PLC," IEEE J. Lightwave Technol., vol.32, no.17, pp.3081–3088, Sept. 2014.
- [10] S. Farwell, P. Aivaliotis, Y. Qian, P. Bromley, R. Griggs, J.N.Y. Hoe, C. Smith, and S. Jones, "InP Coherent Receiver Chip with High Performance and Manufacturability for CFP2 Modules," Proc. OFC/NFOEC 2014, San Francisco, CA, paper W11.6, pp.1–3, March 2014.
- [11] V.E. Houtsma, N. Weimann, T.-C. Hu, R. Kopf, A. Tate, J. Frackoviak, R. Reyes, Y.-K. Chen, C.R. Doerr, L. Zhang, and D. Neilson, "Manufacturable Monolithically Integrated InP Dual-Port Coherent Receiver for 100G PDM-QPSK Applications," Proc. OFC/NFOEC 2011, Los Angeles, CA, paper OML2, pp.1–3, March 2011.
- [12] H. Yagi, N. Inoue, R. Masuyama, T. Kikuchi, T. Katsuyama, Y. Tateiwa, K. Uesaka, Y. Yoneda, M. Takechi, and H. Shoji, "InP-Based p-i-n-Photodiode Array Integrated With 90° Hybrid Using Butt-Joint Regrowth for Compact 100 Gb/s Coherent Receiver," IEEE J. Sel. Topics Quantum Electron., vol.20, no.6, pp.374–380, Nov./Dec. 2014.
- [13] H. Yagi, Y. Yoneda, M. Ekawa, and H. Shoji, "InP-Based Monolithic Integration Technologies for 100/200 Gb/s Pluggable Coherent Transceivers," IEICE Trans. Electron., vol.E100-C, no.2, pp.179–186, Feb. 2017.
- [14] H. Yagi, T. Kaneko, N. Kono, Y. Yoneda, K. Uesaka, M. Ekawa, M. Takechi, and H. Shoji, "InP-Based Monolithically Integrated Photonic Devices for Digital Coherent Transmission," IEEE J. Sel. Topics Quantum Electron., vol.24, no.1, pp.1–11, Jan./Feb. 2018.
- [15] P. Runge, S. Schubert, A. Seeger, K. Janiak, J. Stephan, D. Trommer, P. Domburg, and M.L. Nielsen, "Monolithic InP receiver chip with a 90° hybrid and 56GHz balanced photodiodes," Opt. Express, vol.20, no.26, pp.B250–B255, Nov. 2012.
- [16] A. Matsushita, M. Nakamura, F. Hamaoka, and S. Okamoto, "Transmission Technologies beyond 400-Gbps/carrier Employing High-order Modulation Formats," Proc. European Conference and Exhibition on Optical Communication (ECOC) 2018, Roma, Italy, paper Th1D.1, pp.1–3, Sept. 2018.
- [17] M. Takechi, Y. Tateiwa, M. Kurokawa, Y. Fujimura, H. Yagi, and Y. Yoneda, "64 GBaud High-bandwidth Micro Intradyne Coherent Receiver Using High-efficiency and High-speed InP-based Photodetector Integrated with 90° Hybrid," Proc. OFC/NFOEC 2017, Los Angeles, CA, paper Th1A.2, pp.1–3, March 2017.
- [18] P. Runge, G. Zhou, T. Beckerwerth, F. Ganzer, S. Keyvaninia, S. Seifert, W. Ebert, S. Mutschall, A. Seeger, and M. Schell, "Waveguide Balanced Photodetectors for Coherent Receivers," IEEE J. Sel. Topics Quantum Electron., vol.24, no.2, pp.1–7, March/April 2018.
- [19] M. Kurokawa, M. Takechi, H. Yagi, K. Sakurai, Y. Yoneda, and Y. Fujimura, "High-responsivity L-band Micro Intradyne Coherent Receiver Using InP-based Photodetector Integrated with 90° Hybrid," Proc. SPIE, San Francisco, CA, paper 10561-4, pp.1–6, Jan./Feb. 2018.
- [20] S.-H. Jeong and K. Morito, "Novel Optical 90° Hybrid Consisting of a Paired Interference Based 2×4 MMI Coupler, a Phase Shifter and a 2×2 MMI Coupler," IEEE J. Lightwave Technol., vol.28, no.9, pp.1323–1331, May 2010.
- [21] T. Kikuchi, H. Yagi, N. Inoue, R. Masuyama, T. Katsuyama, K. Uesaka, Y. Yoneda, and H. Shoji, "High-Responsivity of InP-Based

Photodiodes Integrated with 90° Hybrid by Low Excess Loss MMI Design over Wide Wavelength Range,” Proc. 27th IEEE Photonic Conference 2014, San Diego, CA, paper WA4.2, pp.370–371, Oct. 2014.

- [22] T. Okimoto, H. Yagi, R. Masuyama, K. Sakurai, Y. Nishimoto, T. Kikuchi, K. Horino, T. Watanabe, M. Ekawa, M. Takechi, and Y. Yoneda, “Small Responsivity Imbalance of InP-based p-i-n Photodiode Array Monolithically Integrated with 90° Hybrid Using Asymmetric Waveguide Phase Shifter for Coherent Detection,” Proc. Indium Phosphide and Related Materials (IPRM) 2016, Toyama, Japan, paper MoC4-5, pp.1–2, June 2016.
- [23] H. Yagi, N. Inoue, T. Kikuchi, R. Masuyama, T. Katsuyama, Y. Tateiwa, K. Uesaka, Y. Yoneda, M. Takechi, and H. Shoji, “High receiver responsivity and low dark current of InP-based pin-photodiode array monolithically integrated with 90° hybrid and spot-size converter using selective embedding regrowth,” IEICE Electronics Express, vol.12, no.2, pp.1–7, Jan. 2015.
- [24] H. Yagi, N. Inoue, Y. Onishi, R. Masuyama, T. Katsuyama, T. Kikuchi, Y. Yoneda, and H. Shoji, “High-Efficient InP-Based Balanced Photodiodes Integrated with 90° Hybrid MMI for Compact 100 Gb/s Coherent Receiver,” Proc. OFC/NFOEC 2013, Anaheim, CA, paper OW3J.5, pp.1–3, March 2013.
- [25] T. Okimoto, H. Yagi, R. Masuyama, K. Sakurai, Y. Nishimoto, K. Horino, T. Watanabe, M. Ekawa, and Y. Yoneda, “Wide bandwidth and high responsivity of InP-based photodetector monolithically integrated with 90° hybrid for over 400 Gbps coherent transmission systems,” Compound Semiconductor Week (CSW) 2017, Berlin, Germany, paper MoC1-3, pp.1–2, May 2017.



Hideki Yagi received the Ph.D. degree in physical electronics from the Tokyo Institute of Technology, Tokyo, Japan, in March 2004. During his Ph.D. study, he mainly focused on topics of long-wavelength semiconductor lasers based on low-damage and high-uniformity low-dimensional quantum structures. From 2005, he joined Transmission Devices Laboratory, Sumitomo Electric Industries, Ltd., Yokohama, Japan. His research interests are InP-based monolithic integration technologies for coherent

transmission systems and III-V/Si hybrid integration technologies. Dr. Yagi was awarded the best paper award from The 10th Conference on Lasers and Electro-Optics Pacific Rim (CLEO-PR), and The 18th OptoElectronics and Communications Conference (OECC)/ Photonics in Switching 2013 (PS2013). Dr. Yagi is a member of JSAP, IEICE (Senior Member), and IEEE Photonics Society (Senior Member).



Takuya Okimoto received the B.E. and M.E. degrees in electrical engineering from the University of Tokyo, Tokyo, Japan, in 2013 and 2015, respectively. From 2015, he joined Sumitomo Electric Device Innovations, Inc., Yokohama, Japan. He is currently working in InP-based monolithic integration technologies for over 400 Gb/s coherent transmission systems. Mr. Okimoto is a member of JSAP, IEICE, and IEEE Photonics Society.



Naoko Inoue received the M.E. degree in electrical and computer engineering from Yokohama National University, Yokohama, Japan, where she investigated surface-normal-type light control devices in photonic crystals. From 2009, she joined Transmission Devices Laboratory, Sumitomo Electric Industries, Ltd., Yokohama, Japan. She is currently working in InP-based monolithic integration technologies for coherent transmission systems and III-V/Si hybrid integration technologies.



Koji Ebihara received the M.E. degree in electronic engineering from the Tokyo Institute of Technology, Tokyo, Japan, in 2001. In 2001, he joined Fujitsu Laboratories Ltd., Atsugi, Japan, where he has since been engaged in the research and development of high-speed direct modulation semiconductor lasers. In 2003, he moved to Eudyna Devices Inc., Yamanashi, Japan, where he was working on the development of various types of lasers and modulators for optical communication systems. In 2009, he joined Sumitomo Electric Device Innovations, Inc., Yamanashi/Yokohama, Japan. He is currently working on the development of InP-based photonic integrated devices. Mr. Ebihara is a member of JSAP and IEEE Photonics Society.



Kenji Sakurai received the M.E. degree in electronic engineering from the University of Tokyo, Tokyo, Japan, in 2005. In 2005, he joined Transmission Devices Laboratory, Sumitomo Electric Industries, Ltd., Yokohama, Japan. In 2015, he joined Sumitomo Electric Device Innovations, Inc., Yokohama, Japan. He is currently working on the development of InP-based photonic integrated devices. Mr. Sakurai is a member of JSAP, IEICE, and IEEE Photonics Society.



Munetaka Kurokawa received the B.E. and M.E. degrees in electrical and electronic engineering from the Tokyo Institute of Technology, Tokyo, Japan, in 2007 and 2009, respectively. In 2009, he joined Transmission Devices Laboratory, Sumitomo Electric Industries, Ltd., Yokohama, Japan. He is currently working in the development of optical sub-assembly modules.



Satoru Okamoto received the M.E. degree in electrical and electronic engineering from the Kanagawa Institute of Technology, Atsugi, Japan. From 2004 to 2016, he engaged in the development of the magnetic recording head for the hard disk drive at Hitachi Global Storage Technologies Japan, Ltd., and HGST Japan, Ltd. In 2016, he joined Sumitomo Electric Device Innovations, Inc., Yokohama, Japan. He is currently working in the process development of InP-based photonic integrated devices.



Yoshifumi Nishimoto received the M.E. degree in electrical and electronic engineering from the Tokyo Institute of Technology, Tokyo, Japan, in 2007. In 2007, he joined Light transmitting device Division, Sumitomo Electric Industries, Ltd., Yokohama, Japan. In 2009, he joined Sumitomo Electric Device Innovations, Inc., Yokohama, Japan. He is currently working in the process development of InP-based photonic integrated devices.



Kazuhiko Horino received the M.E. degree in interdisciplinary graduate school of science and engineering from the Tokyo Institute of Technology, Yokohama, Japan, in 1992. In 1992, he joined Fujitsu Laboratories Ltd., Atsugi, Japan, where he has since been engaged in the research and development of crystal growth of III-V compound semiconductors. In 2003, he moved to Eudyna Devices Inc., Yamanashi/Yokohama, Japan, where he was working on the development of GaN-based devices.

In 2009, he joined Transmission Devices Laboratory, Sumitomo Electric Industries, Ltd., Yokohama, Japan. He is currently working on the development of InP-based photonic integrated devices as a manager of Sumitomo Electric Device Innovations, Inc. Mr. Horino is a member of JSAP.



Yasuo Yamasaki received the B.E. and M.E. degrees in mechanical engineering from Osaka University, Osaka, Japan, in 1999 and 2001, respectively. In 2001, he joined Sumitomo Electric Industries, Ltd., Yokohama, Japan. From 2008 to 2012, he engaged in the research and development of directly modulated lasers at Transmission Devices Laboratory, Sumitomo Electric Industries, Ltd., Yokohama, Japan. He is currently working on the development of InP-based photonic integrated devices as a manager of Sumitomo Electric Device Innovations, Inc.

of Sumitomo Electric Device Innovations, Inc.



Tatsuya Takeuchi received the M.E. degree in electrical engineering from Kyoto University, Kyoto, Japan, in 1988. In 1989, he joined Fujitsu Laboratories Ltd., Atsugi, Japan, where he was engaged in the research and development of crystal growth of III-V compound semiconductors for optical communication. In 2003, he moved to Eudyna Devices Inc., Yamanashi, Japan, where he was working on the development of semiconductor lasers for optical communication systems. In 2009, he joined

Sumitomo Electric Device Innovations, Inc., Yamanashi/Yokohama, Japan. He is currently working on the development of InP-based photonic integrated devices.



Mitsuru Ekawa received the B.E., M.E., and Ph.D. degrees from Osaka University, Osaka, Japan, in 1987, 1989, and 1993, respectively. During 1989-1993, he worked at the Nagoya Institute of Technology, Nagoya, Japan, to research II-VI compound semiconductors. In 1993, he joined Fujitsu Laboratories Ltd, Atsugi, Japan, where he was engaged in research and development of OMVPE growth of III-V compound semiconductors for optical communication. In 2014, he joined Sumitomo

Electric Industries, Ltd., Yokohama, Japan, where he has been engaged in the development of integrated semiconductor optical devices. Dr. Ekawa is a member of JSAP.



Kouichiro Yamazaki received the M.E. degree in electrical and electronic engineering from Sophia University, Tokyo, Japan, in 2002. In 2002, he joined Transmission Devices Laboratory, Sumitomo Electric Industries, Ltd., Yokohama, Japan. In 2009, he joined Sumitomo Electric Device Innovations, Inc., Yokohama, Japan. He is currently working in the process development of InP-based photonic integrated devices.



Masaru Takechi received the B.E. and M.E. degrees in electronic engineering from the Tokyo Institute of Technology, Tokyo, Japan, in 1984 and 1986, respectively. From 1986 to 2009, he engaged in the research of OMVPE of compound semiconductors and the research and development of optoelectronic devices for optical communication systems at Fujitsu Laboratories Ltd., Fujitsu Ltd., and Eudyna Devices Inc. In 2009, due to the organizational change of Eudyna Devices Inc., he moved to Transmission

Devices Laboratory, Sumitomo Electric Industries, Ltd., Yokohama, Japan, and he is now working on the research and development of intradyne coherent receivers for coherent optical communication systems.



Yoshihiro Yoneda received the B.E. and M.E. degrees from the Nagoya Institute of Technology, Nagoya, Japan, in 1994, and 1996, respectively. In 1996, he joined Fujitsu Laboratories Ltd., Atsugi, Japan, where he has since been engaged in the research and development of high-speed photodetectors. In 2004, he joined Eudyna Devices Inc., Yamanashi/Yokohama, Japan, where he was involved in the development of optoelectronic integrated circuits (OEICs) on InP. In 2009, he joined Sumitomo

Electric Industries, Ltd., Yokohama, Japan. He is currently leading the development of InP-based photonic integrated devices as a group manager of Sumitomo Electric Device Innovations, Inc. Mr. Yoneda is a member of IEICE and IEEE Photonics/Electron Devices Societies.